Photothermal-triggered nanoreactors with tunable catalyst location and catalytic activity

Xiaohui Xu, *[a,b] Radwan M. Sarhan,[a] Shilin Mei, [a] Zdravko Kochovski,[a] Wouter Koopman, [c] Rodney D. Priestley,[b] Yan Lu *[a,d]

[a] Institutue of Soft Matter and Functional Materials, Helmholtz-Zentrum Berlin fur Materialien und Energie, Hahn-Meitner-Platz 1, Berlin, Germany.

[b] Department of Chemical and Biological Engineering, Princeton University, Princeton, New Jersey 08544, United States;

[c] University of Potsdam, Institute of Physics and Astronomy, 14467 Potsdam, Germany

[d] University of Potsdam, Institute of Chemistry, 14467 Potsdam, Germany

* Corresponding author

E-mail: yan.lu@helmholtz-berlin.de

Tel: +49-30-8062-43191

Fax: +49 30 8062-42308

Abstract: Thermosensitive microgels based on poly(N-isopropylacrylamide) (PNIPAm) have been widely used to create nanoreactors with controlled catalytic activity through the immobilization of metal nanoparticles (NPs). However, traditional approaches with the metal NPs located only in the polymer network rely on electric heating to initiate the reaction. In this study, we developed a photothermal-responsive yolk-shell nanoreactor with tunable location of metal NPs. The catalytic performance of these nanoreactors can be controlled by both light irradiation and conventional heating, i.e., electric heating. Interestingly, the location of the catalysts had a significant impact on the reduction kinetics of the nanoreactors: catalysts in the shell exhibited higher catalytic activity compared to those in the core under conventional heating. When subjected to light irradiation, nanoreactors with catalysts loaded in the core demonstrated improved catalytic performance compared to direct heating, while the nanoreactors with catalysts in the shell exhibited relatively similar activity. We attribute this enhancement in catalytic activity to the spatial distribution of the catalysts and the localized heating within the PDA core of the nanoreactors. This research presents exciting prospects for the design of innovative smart nanoreactors and efficient photothermal-assisted catalysis.

Keywords: Near-infrared light, stimuli-responsive, polydopamine, thermoresponsive polymer, catalysis

Introduction

Catalytically active metal nanoparticles (NPs) will aggregate and lose their catalytic properties without proper support.[1, 2] A good support should keep the NPs immobilized and allow for a high density of catalysis centers. Simultaneously, a catalyst support must not inhibit the transport of reactants and products. Microgels are colloidal hydrogel particles with sizes ranging from several nanometers to micrometers.[3-5] Their internal structure, consisting of a swollen gel network, offers ample free space for reactive NPs centers as well as for the flow of reactants and products; thus, making them a viable catalyst support structure.[6] Moreover, microgel supports can be designed to allow for external control over the catalytic process. In particular, stimuli-responsive microgels can undergo volume phase transitions in response to external stimuli, such as temperature, pH, light, or magnetic fields.[7-9] The reversible volume change of these systems can modulate the kinetics of a reaction via the swelling and collapse of the microgel network. Hence, the kinetics of a reaction can be externally controlled.

To date, the most promising smart microgel nanoreactors focus on thermal-responsive systems, such as *polystyrene-poly(N-isopropylacrylamide) (PS-PNIPAm)*[10] or *β-cyclodextrin* modified *poly(N-vinylcaprolactam)*[11] microgels, which incorporate catalytically active nanoparticles (NPs) like Ag, Au, Rh, or Pt into their crosslinked networks. Despite the fact that microgel-based nanoreactors have proven effective in controlling catalytic property, current methods only immobilized catalytically active NPs in the mesh of polymer network *via* hydrogen-bonding or electrostatic interactions. Thus, achieving improved stability of loaded catalysts and superior catalytic performance remains a challenging. Moreover, these nanoreactors are typically controlled through conventional joule heating, which makes the process intrinsically energy-intensive and time-consuming, and increases the probability of side reactions. In contrast, light is naturally abundant, noninvasive, and can be precisely applied to a confined area in a non-contact manner.[12] Thus, light represents an attractive heating source for remotely triggering the phase transition of microgels without physical contact with the system.[13-15] However, achieving light-responsive and controllable localization of catalysts within a single system poses significant challenges.

Herein, we have developed light-responsive nanoreactors capable of controlling the location and catalytic properties of gold nanoparticles (Au NPs) under near-infrared (NIR) light exposure, as shown in (**Fig. 1**). The nanoreactors consist of a shell layer of thermo-responsive PNIPAm grafted atop a photosensitive polydopamine (PDA) core that was precoated with SiO_2 interlayer. By adjusting the addition of a reducing agent, the Au NPs are selectively loaded either into the shell or the core of the microgels during their preparation. Subsequently, the SiO_2 is removed, resulting in a yolk-shell nanoreactor with Au NPs located in different regions. Due to PDA's photosensitive characteristic, the nanoreactor exhibited high photothermal conversion exceeding a temperature of 60 ^{o}C upon light irradiation. Importantly, the introduced PDA microspheres also provide an active surface for the Au NPs *in situ* immobilization without additional reducing agent. We further demonstrated the nanoreactor's ability for catalytic reduction of *p*-Nitroaniline (4-NA), one of the major pollutants generated from industrial processes and pesticide transformation. Additionally, we have investigated the influence of the Au NPs location, whether in the core or the shell of the microgel reactors, on the reaction kinetics.

Results and discussion

Synthesis and characterization of the core-shell microgels. We developed a NIR-light and temperature-controlled catalytic system utilizing photothermal PDA and thermosensitive PNIPAm. The key aspect of our research involves the attachment of a thick and uniform PNIPAm shell onto monodisperse PDA microspheres, which were previously coated with a uniform SiO_2 layer. This resulted in the formation of core-shell microgels termed as PDA-SiO_2-PNIPAm. The inclusion of the silica shell preserves the optical properties of the core material, as it is transparent to light, while also providing C=C double bonds that enable subsequent polymerization.[16] After the polymerization of PNIPAm shell, Au NPs were loaded selectively into either the shell or the core of the prepared microgels. The loading was achieved by using two different methods: reducing B-Au NPs with $NaBH_4$ (referred to as B-Au) or *in situ* reduction using the catechol groups of the PDA core (referred to as P-Au). By controlling the addition of the reducing agent, we successfully produced B-Au@PDA-SiO_2-PNIPAm and P-Au@PDA-SiO_2-PNIPAm microgels with Au NPs located in different regions, as illustrated in **Fig. 1a**.

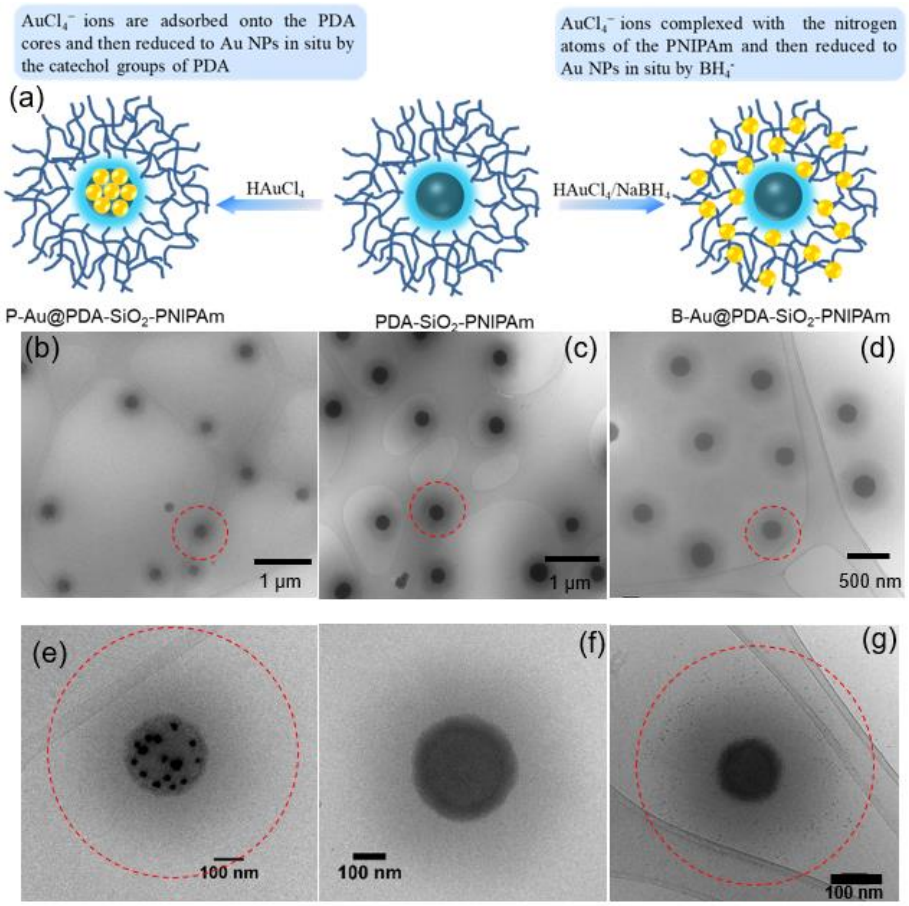

Fig. 1. (a) Schematic illustrating the loading of B-Au NPs and P-Au NPs into microgels. Cryo-TEM images of the P-Au@PDA-SiO_2-PNIPAm nanoreactors (b, e), PDA-SiO_2-PNIPAm microgels (c, f), and B-Au@PDA-SiO_2-PNIPAm nanoreactors (d, g).

To verify the successful synthesis of PDA-SiO_2-PNIPAm microgel, TEM and Cryo-TEM images were employed to characterize the morphologies of the microgels, as displayed in **Fig. 1**. A typical core-shell structure with monodispersed PDA microspheres as the core, a silica interlayer, and PNIPAm polymer as the outer shell was vividly displayed in the TEM images of PDA-SiO_2-PNIPAm (**Fig. S1**). Cryo-TEM images revealed that the well-dispersed PDA-SiO_2-PNIPAm microgels possessed a spherical morphology in the swollen state. The thickness of the PNIPAm shell was about 300 nm (**Fig. 1c, f**). The subsequent immobilization of monodispersed B-Au NPs with an average diameter of < 5 nm into the mesh of the PNIPAm shell was directly visualized in the Cryo-TEM images (**Fig. 1d, g**, **Fig. S2**). The homogeneous and robust immobilization of B-Au NPs was attributed to the strong interaction between metalate ions ($AuCl_4^-$)

with the nitrogen atoms of the PNIPAm shell.[17]

Interestingly, without $NaBH_4$, P-Au NPs appeared in the nanoreactor (**Fig. 1b, e**), but only on the surface of the PDA core (**Fig. S2d**). No additional gold nanoparticles were observed outside the core template (**Fig. S2c**). This is can be attributed to the amino and catechol groups in the PDA, which adsorbed the $AuCl_4^-$ ions and subsequent reduced them to P-Au NPs onto the PDA surface.[18, 19] This method is environmentally friendly as it does not require any additional reducing agent to form P-Au NPs.[2] The point here lies in the distinct positioning of the P-Au NPs within the nanoreactors. This aspect allows for the adjustment of the location, size, and thus the catalytic activity of the Au NPs. Therefore, the PDA component acted as both a light absorber, generating heat, and a modulator, enabling the control of the distribution and size of the Au NPs due to its unique capacity to reduce various metal ions.

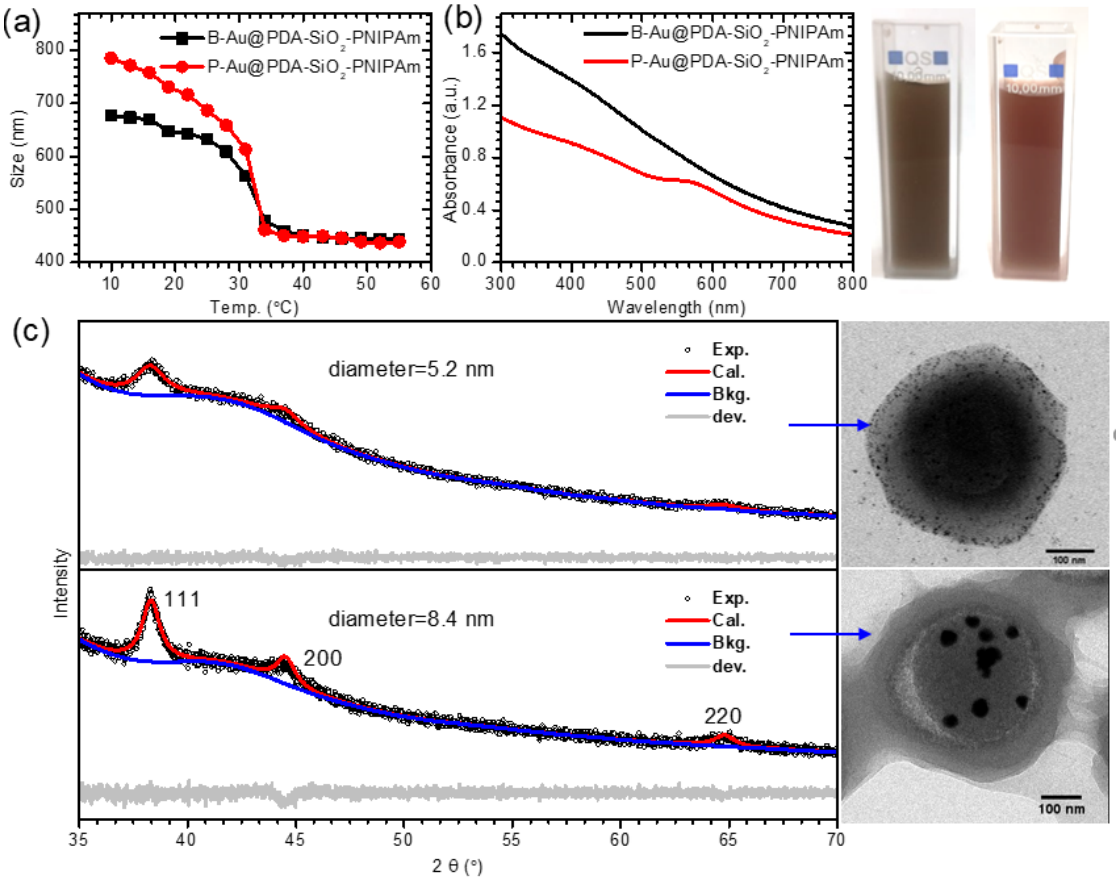

Fig.2. (a) Hydrodynamic diameter changes of microgels at various temperatures. (b) UV-vis absorbance spectra and solution photos. (c) XRD patterns and SEM images of the synthesized microgels loaded with B-Au NPs and P-Au NPs.

The dynamic light scattering (DLS) technique was employed to demonstrate the thermoresponsive characteristic of the PNIPAm shell. **Fig. 2a** illustrates a distinct volume phase transition of the microgels that occurred at approximately 32 °C, attributed to the dehydration of PNIPAm polymer chains and the collapse of the hydrophilic segments.[20] Furthermore, the location of the Au NPs within the core-shell microgels influenced the thermoresponsive behavior of the system at low temperatures. Below the LCST, a reduction in the hydrodynamic radius of B-Au@PDA-SiO_2-PNIPAm was observed in comparison to P-Au@PDA-SiO_2-PNIPAm. This can be attributed to the partial contraction of the PNIPAm network that occurred upon the embedding of B-Au NPs, facilitating amide adsorption with B-Au NPs.

Further proof of the tunable spatial distribution of Au NPs was obtained by UV-vis measurement of the core-shell microgels. The surface plasmon resonance (SPR) absorption of the microgels with different locations of Au NPs is shown in **Fig. 2b**. Compared with the B-Au NPs embedded in the PNIPAm shell (< 5nm in diameter), which have no obvious absorption band of Au NPs, a significantly broadened absorption band at 560 nm was observed for the P-Au NPs, located at the microgel core. This is because P-Au NPs at the core are larger and are closely packed. The tuned spatial distribution of Au NPs accompanies a visible color change of the samples from dark brown to grayish pink (the right image in **Fig. 2b**). We then performed X-ray diffraction (XRD) to further investigate the crystalline structure of B-Au@PDA-SiO_2-PNIPAm and P-Au@PDA-SiO_2-PNIPAm. As shown in the XRD pattern (**Fig. 2c**), the peaks at 38.1°, 44.4°, and 64.8°correspond to the Bragg reflections from (111), (200), and (220) crystalline planes of Au NPs[21], indicating the successful immobilization of Au NPs in the microgels. Moreover, the average size of B-Au and P-Au NPs calculated from the XRD data agreed well with that determined by TEM images.

Formation of nanoreactor with yolk-shell structure. The SiO_2 interlayer plays a crucial role in connecting the PDA core and the PNIPAm shell during the synthesis of the PDA-SiO_2-PNIPAm. However, the presence of the SiO_2 interlayer may decrease heat transfer from the heat source (PDA core) to the surrounding environment due to its relatively low thermal conductivity.[22] Additionally, the SiO_2 interlayer could impede the diffusion rate of reactants to the Au NPs. To address these issues, we eliminated the SiO_2 interlayer using ammonium bifluoride at room temperature (**Fig.**

3a). In this way, a yolk-shell nanoreactor was successfully obtained, as confirmed by the high-resolution cryo-TEM images in **Fig. 3b, c**. The removal of the SiO_2 interlayer did not affect the size (~ 200 nm) and shape of the PDA core, as observed after the etching process. Furthermore, the collapse of the PNIPAm shell eliminated any void space within the yolk-shell nanoreactor. The successful removal of the SiO_2 interlayer was further confirmed through EDX analysis, where the absence of the Si peak was observed after etching (**Fig. 3d**).

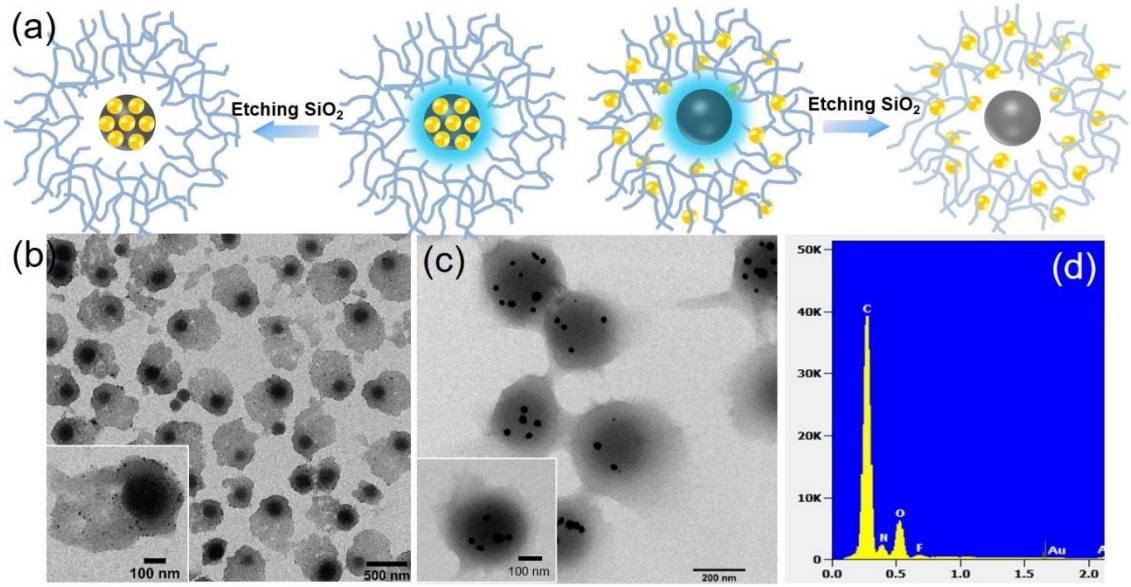

Fig.3. (a) Schematic diagram of the formation of yolk-shell microgels after etching SiO_2, TEM images of (b) B-Au@PDA-PNIPAm and (c) P-Au@PDA-PNIPAm yolk-shell nanoreactors, (d) corresponding EDX to prove the absence of Si element in the P-Au@PDA-PNIPAm.

The long-term durability of nanoreactors is a crucial aspect for their applicability in various fields. To assess their stability, the yolk-shell nanoreactors were immersed in an ammonium hydrogen fluoride solution for a period of three months. The TEM images (**Fig. S3**) revealed that the nanoreactors maintained their physical stability throughout the entire duration. Despite the slow etching of the PDA component under strong alkaline conditions, the particle size of PDA only decreased to a range of 100~150 nm. As a result, the nanoreactors effectively preserved their robust yolk-shell structure, demonstrating excellent stability in practical applications.

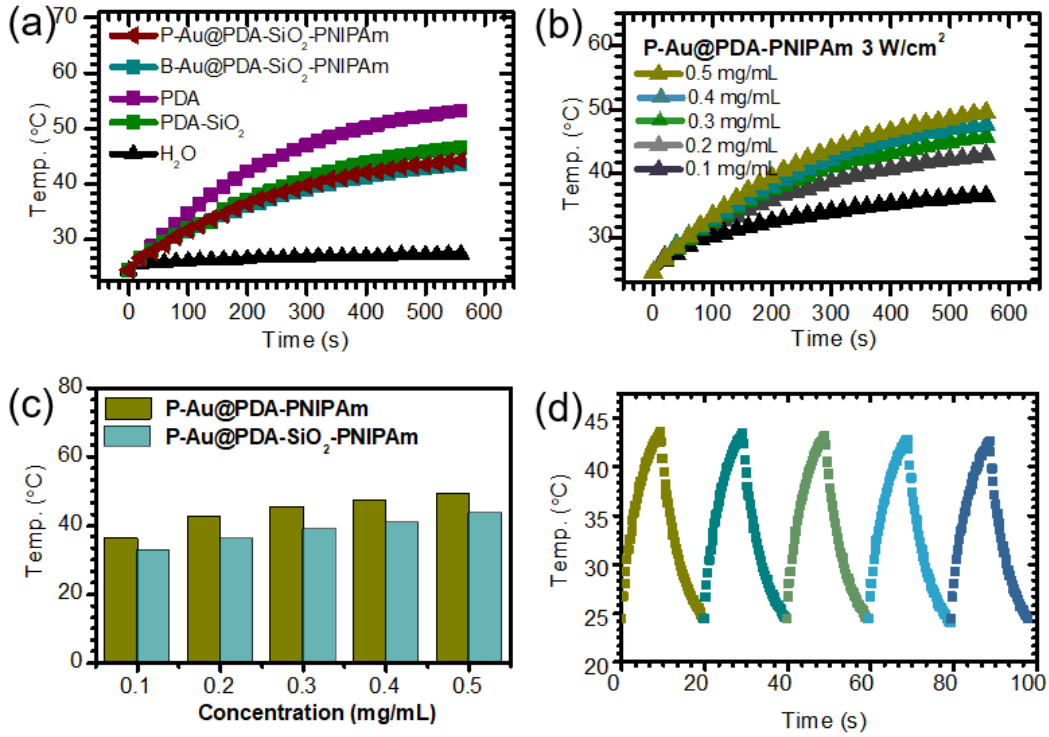

Fig.4. (a) Temperature variation curves of the aqueous dispersions of samples exposed to the 808 nm laser at a power density of 3 W/cm^2. (b) Temperature changes of the P-Au@PDA-PNIPAm. (c) Temperature difference for microgels before and after etching the SiO_2 interlayer. (d) Photostability of the P-Au@PDA-PNIPAm nanoreactor (0.2 mg/mL) with five laser on/off cycles.

Photothermal conversion performance. The nanoreactor facilitates effective conversion of light into heat by PDA, their photothermal conversion efficiency were evaluated under NIR irradiation, as shown in **Fig. 4**. Under continuous laser irradiation (808 nm, 3.0 Wcm^{-2}), the temperature of all the microgel suspensions increase to 53 °C, which exceeds the LCST of PNIPAm (**Fig. 4b**). In contrast, pure water showed only a negligible temperature change under identical irradiation conditions. Notably, after loading of Au NPs, the microgels displayed a relatively lower photothermal conversion effect (T= 43 °C). This implies that the PDA cores play the main role for converting the light energy into thermal energy. Indeed, the laser wavelength of 808 nm was chosen, such to ensure a vanishing direct absorption of light by the Au NPs. Moreover, the Au NPs are too small to show plasmonic absorption. As a result, microgels with B-Au and P-Au NPs exhibited similar temperature increase during illumination, thus, showing that the locations of the catalytic NPs did not affect heat generation.

The nanoreactor enables efficient conversion of light into heat through PDA.[23-25] The

photothermal conversion efficiency of the nanoreactor was evaluated using near-infrared (NIR) irradiation, as depicted in **Fig. S4**. When exposed to continuous laser irradiation (808 nm, 3.0 Wcm^{-2}), the temperature of all suspensions increased quickly and surpassed the LCST of PNIPAm (**Fig. 4a**). In contrast, pure water exhibited negligible temperature change under the same irradiation conditions. Importantly, the introduction of Au NPs into the microgels resulted in a relatively lower photothermal conversion effect (T= 43 °C). This suggests that the PDA cores are primarily responsible for converting light energy into thermal energy. The choice of 808 nm laser wavelength ensures minimal direct absorption of light by the Au NPs, which are also too small to exhibit plasmonic absorption. Consequently, microgels containing B-Au and P-Au NPs demonstrated similar temperature increases during illumination, indicating that the positions of the catalytic NPs did not affect heat generation.

In the case of the nanoreactor suspension, the temperature increased from 35.7 to 49.1 °C with concentrations ranging from 0.1 to 0.5 mg mL^{-1}(**Fig.4b**). The yolk-shell nanoreactors exhibited a greater temperature rise under NIR irradiation compared to core-shell microgels with a SiO_2 interlayer (**Fig.4c**). This enhanced photothermal conversion is advantageous for the catalytic reaction. Furthermore, the nanoreactors exhibited a stable temperature response when the NIR laser irradiation was turned on and off repeatedly (**Fig.4d**). It should be noted that the removal of the SiO_2 interlayer in the yolk-shell microgels did not suppress the volume shrinkage behavior at high temperatures (**Fig.S6**). Given the superior photothermal performance and improved accessibility for reactants, we focus on the yolk-shell structure in the subsequent analysis.

Photo- and temperature-responsive catalytic activity. A core functionality of "smart" microgel nanoreactors is their ability to regulate the catalytic activity of the incorporated metal NPs through the volume transition of the polymer network.[26] As yolk-shell nanoreactors, the catalytic kinetics of B-Au@PDA-PNIPAm and P-Au@PDA-PNIPAm were investigated on the catalytic reduction of 4-NA. We chose 4-NA is because it is an aromatic amine extensively used as an intermediate in the production of various pesticides[27] Thus, it is a pervasive contaminant in the environment, particularly in agricultural soil due to the extensive global use of pesticides (roughly 2 million tons per year[28]). In addition, the reaction product is *p*-phenylenediamine (4-PA), which is an important industrial intermediate for the commercial preparation of many organic compounds including

polymers, azo dyes, fur dyes and rubber antioxidants.

The kinetics of this reaction can be easily monitored by UV-vis spectroscopy (**Fig.5a**). With nanoreactors, the peak of 4-NA centered at ~379 nm, gradually decreases with time, and a new band appears at ~240 nm due to the formation of 4-PA[29]. The light-induced reduction of 4-NA follows pseudo first-order kinetics. Hence, k_{app} was directly obtained from the linear slope of $ln(A_t/A_0)$ versus the reaction time t (**Fig.S7-8**). To compare the photocatalytic activity of different systems directly, we employed the surface reaction rate k_1, i.e., the experimentally measured apparent rate constant (k_{app}) normalized to the theoretical specific metal particle surface area of the Au NPs. As we showed in a previous article,[17] this normalized quantity can be directly linked to the catalytic properties of a single particle. It is worth noting that in all experiments, the light solely did not initiate the reaction in absence of $NaBH_4$, which suggests a minor role of the plasmon-generated energetic electrons.

As shown in **Fig. 5b**, reaction rates were influenced dramatically by the environmental temperature. The rate constants k_1 obtained at different temperatures for B-Au@PDA-PNIPAm and P-Au@PDA-PNIPAm nanoreactors did not follow the typical Arrhenius-type dependence on temperature. We attribute this behavior to the strong temperature dependence of the overall volume of the PNIPAm network, which affects the catalytic efficiency of the nanoreactor. At low temperature, the network is fully swollen, facilitating the diffusion of the reactant molecules (4-NA) onto the catalyst surface. The reaction rate therefore increases when increasing the temperature and showed a local maximum around 25 °C. However, when the reaction temperature exceeds 25 °C, the polymer network undergoes substantial shrinkage, impeding the diffusion of reactants within the network. This leads to a decrease in the rate constant, resulting in a local minimum at 32.5 °C (the LCST of the PNIPAm shell), which is similar with the result obtained for metal nanoparticles immobilized in microgels.[17] Further increases in temperature do not result in additional shrinking of the PNIPA network. At this point, the significant increase of k_1 with T surpasses the hindered diffusion and thus the reaction rate rises again. These findings confirm that the catalytic activity of our nanoreactors can be modulated by the volume transition of the carrier system at different temperatures.

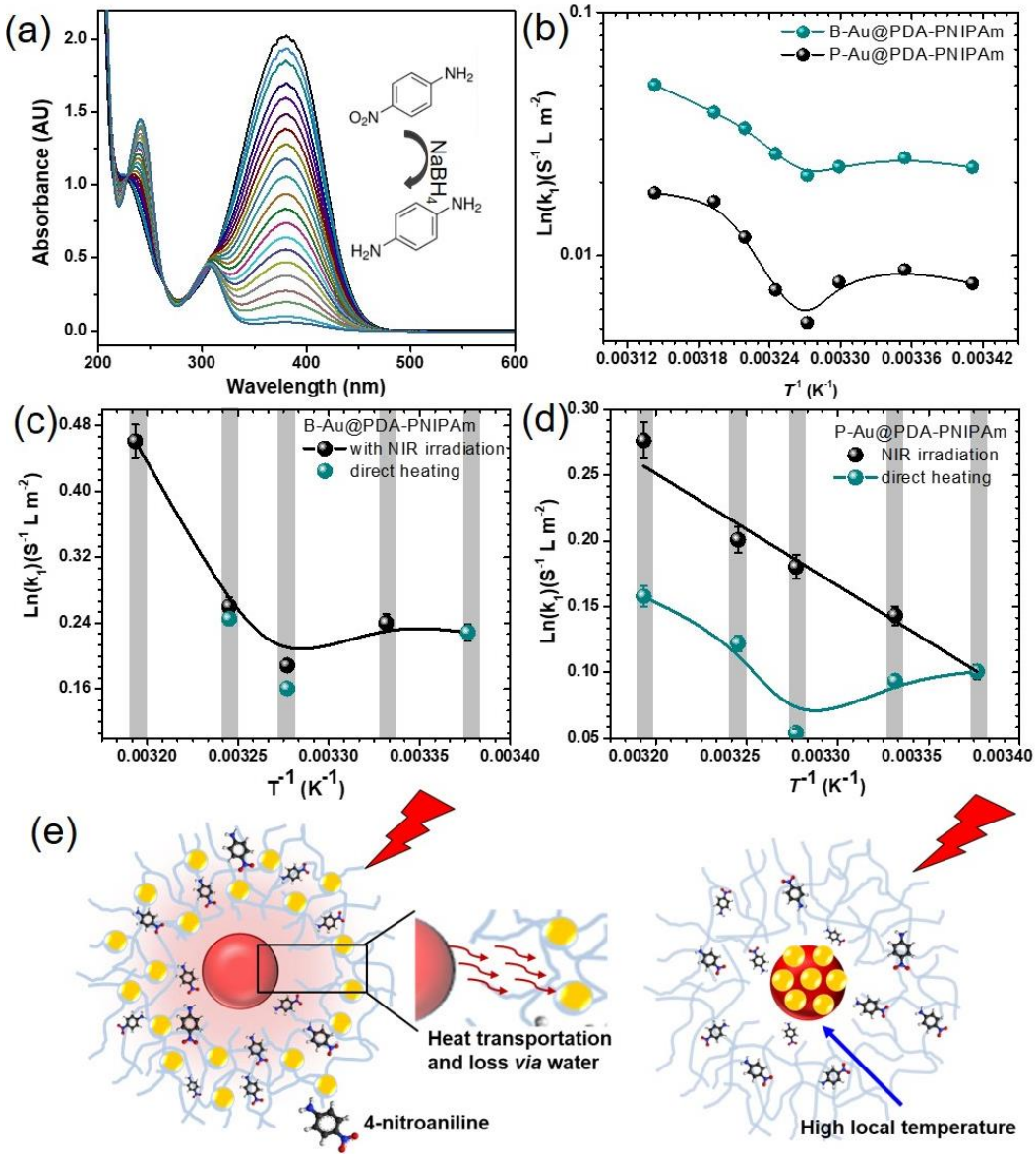

Fig.5. (a) UV-vis spectra of the reduction reaction of 4-NA by sodium borohydride using B-Au@@PDA-PNIPAm. (b) The reaction rate k_1 (rate constant k_{app} normalized to the surface area of B-Au and P-Au NPs) at different temperatures. Catalytic activity of B-Au@PDA-PNIPAm (c) and P-Au@PDA-PNIPAm (d) under NIR irradiation with different power densities and under direct heating (red dots) to various temperatures. The concentrations are as follows: [4-NA] = 1.6 mM, [$NaBH_4$] = 160 mM, [microgels] = 0.2 g L^{-1}. (e) Illustration of the catalytic process of P-Au NPs in the core and B-Au NPs in the shell of nanoreactors under NIR light irradiation.

The combination of a photothermal agent (PDA) and a thermosensitive polymer (PNIPAm) within a single nanoplatform presents an approach for controlling the catalytic activity of metal nanoparticles using remote light. This eco-friendly method serves as an alternative to conventional

heating. To investigate the remote control of the catalytic performance, we examined the reaction rates of the 4-NP reduction while illuminating the nanoreactors with NIR light at different intensities. The reaction rate in B-Au@PDA-PNIPAm exhibited a non-Arrhenius trend, similar to the observations made when externally heating the system with a heater (**Fig. 5c**). In the absence of NIR irradiation, the temperature of the nanoreactor solution remained at 23±0.2°C, and the PNIPAm network of the nanoreactors remained in a swollen state. However, upon applying a laser intensity of 2.4 W/cm^2, the nanoreactor dispersion was heated to 32±0.5°C (the LCST), benefiting from the photothermal conversion of the PDA cores (**Fig.S9**). Consequently, the PNIPAm shell of B-Au@PDA-PNIPAm experienced significant shrinkage, leading to a deceleration in the diffusion of reactants into the catalyst embedded within the shell, subsequently resulting in a decrease in the reaction rate. As we further increased the laser intensity, the reaction rate began to increase again due to the elevated temperature.

In contrast to the B-Au@PDA-PNIPAm nanoreactors, the P-Au@PDA-PNIPAm nanoreactors exhibited a significantly slower reaction rate. This difference can be ascribed to the presence of P-Au NPs confined within the yolk, making them less accessible in general. Moreover, light-intensity dependence of the reaction rate unexpectedly displayed a linear trend, indicating a temperature-limited Arrhenius-type process. This is markedly different from the trend observed upon direct heating or using the B-Au@PDA-PNIPAm (**Fig. 5d**) and must be directly related to the placement of the catalytic metal particles within the PDA yolk. We believe that this behavior is a result of the localized heat production in core of the nanoreactors. The unique P-Au locations (active reaction sites) on the PDA cores directly utilize the local heat surrounding the PDA, which make the surface temperature of the Au and PDA higher than the bulk solution (**Fig. 5e**, **Fig.S10**). We believe that this temperature rise is sufficient to shrink the particle. Hence, it converts the diffusion-dominated behavior into a temperature-dominated behavior, which explains the linear dependence of the reaction rate on the temperature in the present study as shown **in Fig. 5d**. Overall, we showed that our PDA-based smart nanoreactors control the catalytic performance in multiple ways, where the photothermal effect as well as the resulting thermal gradient play the dominant role.

Conclusions

In summary, we have developed photothermal responsive nanoreactors with a yolk-shell structure with control of the location of catalysts. The nanoreactors consist of a PDA core, a PNIPAm shell, and Au NPs acting as catalysts for the reduction of *p*-Nitroaniline. The selective location of Au NPs within the shell or on the PDA cores allows them to function as reductants and stabilizers for in-situ generation of Au NPs. The microgels exhibit efficient photoheating capabilities and long-term colloidal stability, even in the presence of strong base conditions. The catalytic activity of B-Au in the shell can be adjusted by the volume transition of the thermosensitive shell under light irradiation, showing a similar trend to the catalytic reaction under heating. On the other hand, the catalytic reaction rate of P-Au located on top of PDA demonstrates improved activity under near-infrared (NIR) light, despite the significant shrinkage of the PNIPAm shell. This indicates that the reaction kinetics are primarily temperature-dependent rather than dominated by diffusion. Overall, this work provides new possibilities for the design of light-responsive nanoreactors, expanding their applications in catalysis, photothermal therapy, drug delivery systems, bioengineering, and medical therapy.

Experimental section

Materials. 3-hydroxytyramine hydrochloride (dopamine), tetrachloroaurate hydrate ($HAuCl_4 \cdot 4H_2O$), *N*-isopropylacrylamide (NIPAm), *N,N*′-methylenebisacrylamide (MBA), tetraethyl orthosilicate (TEOS), 3-(trimethoxysilyl)propyl methacrylate (MPS), *p*-Nitroaniline (4-NA), poly(vinylpyrrolidone) (Mw=29000, PVP), ammonium hydrogen fluoride, sodium hydroxide ($NaBH_4$) and potassium persulfate (KPS) were supplied by Sigma Aldrich and used as received.

Preparation of surface-functionalized PDA-SiO2 microgels. For the preparation of PDA microspheres,[30] 2.0 mL of 28-30% NH_4OH, 40 mL of ethanol, and 90 mL of deionized water were added to a 250 mL Erlenmeyer flask, followed by addition of dopamine hydrochloride (1.0 g). After stirring at room temperature for 24 h, the color of the solution became brownish black due to the formation of PDA microspheres. The PDA microspheres were washed with water and

dispersed into 79.8 mL ethanol, followed by addition of 4.6 mL of NH_4OH and 0.5mL of TEOS under continuous stirring. The reaction mixture was left at 20 °C for 6 h to ensure complete coating of SiO_2 interlayer around PDA cores. The PDA-SiO_2 surface was functionalized by 3-(trimethoxysilyl)propylmethacrylate (MPS, 8.6 mL), and the solution was maintained at 80 °C for 36 h. In the end, the surface-functionalized PDA-SiO_2 nanoparticles were washed by centrifugation (5500 rpm, 12 min) and re-dispersed in ethanol (5.0 mL).

Preparation of the PDA-SiO2-PNIPAm core-shell microgel. PDA-SiO_2-PNIPAm core-shell microgels were synthesized *via* seeded emulsion polymerization.[16] Typically, 0.6 mL of surface-functionalized PDA-SiO_2 nanoparticles in ethanol was dispersed in 12 mL of poly(vinylpyrrolidone) (Mw = 29000 PVP) aqueous solution. After stirring for 15 min at 35°C, 4.0 mL of water containing NIPAm (0.24 g) and MBA (0.016 g) was added into the mixed solution. The mixture was heated to 80 °C under a nitrogen atmosphere and the polymerization started by the addition of 4.8 mg KPS (dissolved in 1 mL water). The brown solution became grayish white after 15 min and the reaction was lasted for 4 h at 70 °C. The composite particles were then cleaned by serum replacement against deionized water (cellulose nitrate membrane, 100 nm pore size) and dispersed in water.

Deposition of metal nanoparticles in microgels. In a typical process, 100 mg of microgels were dispersed in 100 mL of distilled water and stirred for 30 min in an ice bath. Subsequently, 1 mL of 0.01 M $HAuCl_4$ was added and stirred for 1 h. After being degassed with nitrogen for 30 min, 10 mL of 0.15 M ice-cold sodium borohydride solution was added at once and the mixture was kept for another 30 min with stirring. In this way, gold nanoparticles reduced by BH_4^- (denoted as B-Au) were implemented in the shell of the B-Au@PDA-SiO_2-PNIPAm nanoreactors. Additionally, $AuCl_4^-$ can be reduced by PDA into P-Au NPs. Therefore, P-Au@PDA-SiO_2-PNIPAm nanoreactors were prepared according to the same procedures described above without additional reducing agent. After centrifugation, the as-prepared nanoreactors were washed with distilled water and the precipitate was freeze-dried for 12 h. The amount of loaded Au NPs was subsequently measured by TGA analysis. To determine the impact of silica interlayer on the photothermal effect, yolk-shell microgels were prepared by a silica-etching procedure: 0.1 g of microgels was added into NH_4HF_2 (25 mL, 2M) solution. The mixture was gently stirred at room temperature overnight and was cleaned by centrifugation (5000 rpm, 10 min).

Measurement of photothermal performance. For measuring the photothermal conversion performance, 1mL of suspension with various concentrations (0-0.5mg/mL) were placed into quartz cuvettes and irradiated with a NIR laser (λ = 808 nm) for 10 min. Meanwhile, an infrared thermometer monitored the temperature variation of the dispersions at each time interval. As a control, we measured the temperature increase in 1 mL of distilled water.

Temperature- and light-responsive catalytic activity test. To evaluate the thermo-responsive catalytic reduction of *p*-Nitroaniline (4-NA), sodium borohydride solution (0.4 mL) was added to a 4-NA solution (2.5 mL, 0.2 mM) contained in a glass vessel and agitated at different temperature from 20 to 45 °C. The solution was purged with N_2 to remove the oxygen from the system. Thereafter, a given amount of B-Au@PDA-PNIPAm (0.1 mL, 0.12 mg/mL) or P-Au@PDA-PNIPAm (0.02 mL, 3.47 mg/mL) was added. Immediately after the addition of microgels, UV-vis spectra of the sample were taken every 1 min in the wavelength range of 250-500 nm. Catalytic reduction of 4-NA in an aqueous media under NIR light irradiation: 0.2 mL of B-Au@PDA-PNIPAm or P-Au@PDA-PNIPAm were suspended into 0.8 mL of 4-NA solution (2 mM) and the solution was exposed to the 808 nm NIR light at different laser powers. Immediately after the addition of the sodium borohydride solution (0.1 mL), 0.1 mL of the supernatants was collected and diluted to 2 mL at predetermined time to analyze the UV-vis spectra. During the catalytic process, the temperature of the solution was recorded by thermocouple thermometer.

Sample analysis. The hydrodynamic diameters of the thermosensitive microgels were determined by dynamic light scattering (Malvern Zetasizer Nano ZS ZEN 3500). The core-shell and yolk-shell structures were examined using a JEOL JEM-2100 transmission electron microscope (TEM) and cryogenic transmission electron microscopy (Cryo-TEM) operating at an acceleration voltage of 300 kV. The size distribution of Au nanoparticles in the microgels were measured using Image J software from their TEM images. UV−vis-NIR spectra were obtained using a Lambda 650 spectrophotometer supplied by PerkinElmer. X-ray diffraction patterns (XRD) of microgel composites were obtained from a in a Bruker D8 diffractometer with Cu Kα radiation (0.05°/min scan rate). The photothermal performance was evaluated using an 808 nm laser (0-5 W/cm^2, Changchun New Industries Optoelectronics Tech. Co., Ltd), and the temperature change was recorded by a thermocouple thermometer (WH380, WHDZ).

AUTHOR INFORMATION

Corresponding Author

*Tel: +49-30-8062-43191Fax: +49 30 8062-42308Email: yan.lu@helmholtz-berlin.de.

Notes The authors declare no competing financial interest.

Reference

1. Kwiczak-Yiğitbaşı, J.; Laçin, Ö.; Demir, M.; Ahan, R. E.; Şeker, U. Ö. Ş.; Baytekin, B. A sustainable preparation of catalytically active and antibacterial cellulose metal nanocomposites via ball milling of cellulose. *Green Chemistry* **2020,** *22* (2), 455-464.

2. Xu, X.; Sun, L.; Bai, B.; Wang, H.; Suo, Y. Interfacial assembly of mussel-inspired polydopamine@ Ag core–shell nanoparticles as highly recyclable catalyst for nitroaromatic pesticides degradation. *Science of The Total Environment* **2019,** *665*, 133-141.

3. Myrick, J. M.; Vendra, V. K.; Le, N.-T.; Sexton, F. A.; Krishnan, S. Controlled release of glucose from orally delivered temperature-and pH-responsive polysaccharide microparticle dispersions. *Industrial & Engineering Chemistry Research* **2019,** *58* (46), 21056-21069.

4. Zhang, R.; Xiang, B.; Shen, Y.; Xia, L.; Xu, L.; Guan, Q.; Tang, S. Energy-efficient smart window based on a thermochromic microgel with ultrahigh visible transparency and infrared transmittance modulation. *Journal of Materials Chemistry A* **2021,** *9* (32), 17481-17491.

5. Wang, M.; Gao, Y.; Cao, C.; Chen, K.; Wen, Y.; Fang, D.; Li, L.; Guo, X. Binary solvent colloids of thermosensitive poly (N-isopropylacrylamide) microgel for smart windows. *Industrial & Engineering Chemistry Research* **2014,** *53* (48), 18462-18472.

6. Zhang, Y.; Liu, P.; Li, B.-G.; Wang, W.-J. CO2-Triggered Recoverable Metal Catalyst Nanoreactors using Unimolecular Core–Shell Star Copolymers as Carriers. *ACS Applied Nano Materials* **2018,** *1* (3), 1280-1290.

7. Zha, L.; Banik, B.; Alexis, F. Stimulus responsive nanogels for drug delivery. *Soft Matter* **2011,** *7* (13), 5908-5916.

8. Sala, R. L.; Goncalves, R. H.; Camargo, E. R.; Leite, E. R. Thermosensitive poly (N-vinylcaprolactam) as a transmission light regulator in smart windows. *Solar Energy Materials and Solar Cells* **2018,** *186*, 266-272.

9. Wang, Y.; Zhang, Y.; Guan, Y.; Zhang, Y. Magnetic Field-Assisted Fast Assembly of Microgel Colloidal Crystals. *Langmuir* **2022**.

10. Mei, Y.; Lu, Y.; Polzer, F.; Ballauff, M.; Drechsler, M. Catalytic activity of palladium nanoparticles encapsulated in spherical polyelectrolyte brushes and core− shell microgels. *Chemistry of Materials* **2007,** *19* (5), 1062-1069.

11. Jia, H.; Schmitz, D.; Ott, A.; Pich, A.; Lu, Y. Cyclodextrin modified microgels as “nanoreactor” for the generation of Au nanoparticles with enhanced catalytic activity. *Journal of Materials Chemistry A* **2015,** *3* (11), 6187-6195.

12. J.Gaitzsch, X. H., B.Voit. Engineering Functional Polymer Capsules toward Smart Nanoreactors. *Chemical Reviews* **2015,** *116* (3), 1053.

13. Li, S.; Lin, D.; Zhou, J.; Zha, L. Preparation of silver nanoparticles loaded photoresponsive composite microgels and their light-controllable catalytic activity. *The Journal of Physical Chemistry C* **2016,** *120* (9), 4902-4908.

14. Li, M.-H.; Keller, P. Stimuli-responsive polymer vesicles. *Soft Matter* **2009,** *5* (5), 927-937.

15. Alvarez‐Lorenzo, C.; Bromberg, L.; Concheiro, A. Light‐sensitive intelligent drug delivery systems. *Photochemistry and photobiology* **2009,** *85* (4), 848-860.

16. Wu, S.; Dzubiella, J.; Kaiser, J.; Drechsler, M.; Guo, X.; Ballauff, M.; Lu, Y. Thermosensitive Au‐PNIPA yolk–shell nanoparticles with tunable selectivity for catalysis. *Angewandte Chemie International Edition* **2012,** *51* (9), 2229-2233.

17. Lu, Y.; Yuan, J.; Polzer, F.; Drechsler, M.; Preussner, J. In situ growth of catalytic active Au− Pt bimetallic nanorods in thermoresponsive core− shell microgels. *Acs Nano* **2010,** *4* (12), 7078-7086.

18. Wang, D.; Bao, L.; Li, H.; Guo, X.; Liu, W.; Wang, X.; Hou, X.; He, B. Polydopamine stabilizes silver nanoparticles as a SERS substrate for efficient detection of myocardial infarction. *Nanoscale* **2022,** *14* (16), 6212-6219.

19. Yang, H.; Zhao, X.; Zhang, Z.; Ma, P.; Wang, X.; Song, D.; Sun, Y. Biotin-streptavidin sandwich integrated PDA-ZnO@ Au nanocomposite based SPR sensor for hIgG detection. *Talanta* **2022,** *246*, 123496.

20. Zhelavskyi, O. S.; Kyrychenko, A. Atomistic molecular dynamics simulations of the LCST conformational transition in Poly (N-Vinylcaprolactam) in water. *Journal of Molecular Graphics and Modelling* **2019**.

21. Liu, G.; Wang, D.; Zhou, F.; Liu, W. Electrostatic self‐assembly of Au nanoparticles onto thermosensitive magnetic core‐shell microgels for thermally tunable and magnetically recyclable catalysis. *Small* **2015,** *11* (23), 2807-2816.

22. Gao, M.; Peh, C. K.; Phan, H. T.; Zhu, L.; Ho, G. W. Solar Absorber Gel: Localized Macro‐Nano Heat Channeling for Efficient Plasmonic Au Nanoflowers Photothermic Vaporization and Triboelectric Generation. *Advanced Energy Materials* **2018,** *8* (25), 1800711.

23. Chen, W.; Miao, H.; Meng, G.; Huang, K.; Kong, L.; Lin, Z.; Wang, X.; Li, X.; Li, J.; Liu, X. Y. Polydopamine‐Induced Multilevel Engineering of Regenerated Silk Fibroin Fiber for Photothermal Conversion. *Small* **2022,** *18* (11), 2107196.

24. Liu, Y.; Liu, H.; Xiong, J.; Li, A.; Wang, R.; Wang, L.; Qin, X.; Yu, J. Bioinspired design of electrospun nanofiber based aerogel for efficient and cost-effective solar vapor generation. *Chemical Engineering Journal* **2022,** *427*, 131539.

25. Zhang, X.; Pi, M.; Lu, H.; Li, M.; Wang, X.; Wang, Z.; Ran, R. A biomass hybrid hydrogel with hierarchical porous structure for efficient solar steam generation. *Solar Energy Materials and Solar Cells* **2022,** *242*, 111742.

26. Lu, Y.; Proch, S.; Schrinner, M.; Drechsler, M.; Kempe, R.; Ballauff, M. Thermosensitive core-shell microgel as a “nanoreactor” for catalytic active metal nanoparticles. *Journal of Materials Chemistry* **2009,** *19* (23), 3955-3961.

27. Khan, F.; Pandey, J.; Vikram, S.; Pal, D.; Cameotra, S. S. Aerobic degradation of 4-nitroaniline (4-NA) via novel degradation intermediates by Rhodococcus sp strain FK48 (vol 254, pg 72, 2013)(Retraction of Vol 254, Pg 72, 2013). *Journal of hazardous materials* **2017,** *340*, 486-486.

28. Galli, A.; De Souza, D.; Machado, S. A. Pendimethalin determination in natural water, baby food and river sediment samples using electroanalytical methods. *Microchemical Journal* **2011,** *98* (1), 135-143.

29. Jakhmola, A.; Celentano, M.; Vecchione, R.; Manikas, A.; Battista, E.; Calcagno, V.; Netti, P. Self-assembly of gold nanowire networks into gold foams: production, ultrastructure and applications.

Inorganic Chemistry Frontiers **2017,** *4* (6), 1033-1041.

30. Liu, Y.; Ai, K.; Liu, J.; Deng, M.; He, Y.; Lu, L. Dopamine‐melanin colloidal nanospheres: an efficient near‐infrared photothermal therapeutic agent for in vivo cancer therapy. *Advanced materials* **2013,** *25* (9), 1353-1359.